










Soft glass optical fiber characterization with X-ray computed microtomography

MARIA C. CROCCO,^{1,2} FABIO MANGINI,³  RAFFAELE FILOSA,^{1,2} ANDREA SOLANO,^{1,4} RAFFAELE G. AGOSTINO,^{1,2,5} RICCARDO C. BARBERI,^{1,2,5}  VINCENT COUDERC,⁶  MARIUSZ KLIMCZAK,⁷  ADAM FILIPKOWSKI,^{7,8} RYSZARD BUCZYNSKI,^{7,8}  STEFAN WABNITZ,^{3,9}  VINCENZO FORMOSO,^{1,2,5} AND MARIO FERRARO^{1,2,3,*} 

¹STAR Research Infrastructure, University of Calabria, Via Tito Flavio, 87036 Rende (CS), Italy

²Department of Physics, University of Calabria, Via P. Bucci, 87069 Rende, Italy

³Department of Information Engineering, Electronics and Telecommunications, Sapienza University of Rome, Via Eudossiana 18, 00184 Rome, Italy

⁴Department of Computer Engineering, Modeling, Electronics and Systems, University of Calabria, Via P. Bucci, 87069 Rende, Italy

⁵CNR Nanotec, Via P. Bucci, 87069 Rende, Italy

⁶XLIM, UMR CNRS 7252, University of Limoges, 123 Avenue A. Thomas, 87060 Limoges, France

⁷Faculty of Physics, University of Warsaw, Pasteura 5, 02-093, Warsaw, Poland

⁸Lukasiewicz Research Network - Institute of Microelectronics and Photonics, Al. Lotnikow 32/46, 02-668, Warsaw, Poland

⁹CNR-INO, Istituto Nazionale di Ottica, Via Campi Flegrei 34, 80078 Pozzuoli, Italy

*mario.ferraro92@unical.it

Abstract: The high loss due to the presence of strong phonon resonances makes silica fibers unfit for applications in the mid-infrared spectral range. This has led to the development of specialty optical fibers, based on novel materials and manufacturing techniques. In some cases, the characterization of these new fibers by means of standard techniques may be challenging. Fiber manufacturers would strongly benefit from a tool, which is capable of checking the geometrical and optical properties of fibers (either after fiber drawing, or even in real-time, during the drawing process). Here, we propose and demonstrate that absorption contrast X-ray computed microtomography is a non-destructive technique, capable of characterizing both geometrical and optical properties of specialty optical fibers. We experimentally verified that the tomographic intensity profile in the fiber core has the same shape as the refractive index profile, which we determined via energy-dispersed X-ray spectroscopy. We tested step- and graded-index soft glass fibers, both purchased and made in-house. Owing to the presence of high atomic number elements, which provide higher X-ray cross-section, soft glasses were more suitable than silica for their characterization via X-ray computed microtomography.

© 2023 Optica Publishing Group under the terms of the [Optica Open Access Publishing Agreement](#)

1. Introduction

Nowadays, the use of optical fiber-based technologies is widely adopted in a variety of applications, ranging from optical communication networks, material processing and micro-machining, to biomedical imaging. The waveguiding properties of optical fibers, i.e., their capability of tightly confining light along the directions orthogonal to the fiber axis, are mainly due to the different refractive indexes of their core and cladding. The most effective manufacturing technique of standard fibers, i.e., made of silica, is chemical vapor deposition (CVD) [1]. CVD allows for finely tuning the chemical composition of the fiber core and cladding, which can be doped with different elements and concentrations. For instance, commercially available fibers are either made

of pure silica core and fluorine-doped cladding, or of pure silica cladding and germanium-doped core. As a matter of fact, fluorine (germanium) doping produces a decrease (increase) of the refractive index (n) of silica [2]. Therefore, one may retrieve the refractive index profile by tracing the content of the dopant via energy-dispersed X-ray spectroscopy (EDX), i.e., by analyzing the characteristic X-ray emission which is produced by the absorption of electrons having the energy of the order of a few keV. As a matter of fact, electron spectroscopes, such as EDX, are particularly effective when dealing with low atomic number (Z) materials, such as silica.

CVD permits a fine-tuning of the chemical composition of the fiber component materials, so that one may obtain arbitrary shapes of the refractive index. Indeed, besides abrupt variations of the chemical composition of the core and cladding, which give rise to the so-called step-index refractive index profile, one may obtain smooth variations of the chemical composition at the core/cladding interface. For instance, the so-called graded-index (GRIN) fibers have a parabolic refractive index profile inside the fiber core, which may even be continuous at the core/cladding interface. Thanks to their parabolic shape of the refractive index, GRIN fibers have unique optical properties, e.g., the mitigation of modal dispersion, and equal spacing of the mode propagation constants, which leads to the phenomenon of spatial self-imaging [3]. The latter represents an outstanding resource for many applications, e.g., it leads to frequency conversion via geometric parametric instability [4] and it strongly facilitates the so-called spatial beam self-cleaning effect [5].

Silica optical fibers permit to operate in a relatively wide range of the electromagnetic spectrum, depending on their OH content. In particular, silica can be treated to have either high (i.e., of about several hundred ppm) or low (i.e., less than a few ppm) OH content. In the former case, the material is transparent in the ultraviolet spectral range, and it may exhibit solarization-resistant properties [6], whereas, in the latter, silica fibers are used for near-infrared (IR) applications, e.g., for telecommunications [7].

At even longer wavelengths, i.e., when operating in the mid-IR spectral range, silica is characterized by a strong linear absorption [7], owing to its pronounced phonon resonances. As such, regardless of the manufacturing technique, silica fibers are intrinsically unfit for applications at mid-IR frequencies, e.g., for gas monitoring [8], molecular fingerprinting [9], and biomedicine [10], to cite a few. In this spectral range, non-silica materials with negligible optical losses are commonly used [11]. It is mainly for this reason that non-silica fibers have been targeted for broadband spectrum applications, such as those based on supercontinuum generation mechanisms [12].

Non-silica fibers are often referred to as specialty optical fibers. Generally speaking, the materials for mid-IR fiber optics are soft glasses, mostly fluoride, and germanate glasses doped with high Z elements, such as lead, bismuth, and rare-earths. However, at variance with silica, soft glasses are less resistant to mechanical stresses and break more easily.

To date, virtually all commercial soft glass fibers have step-index profiles. However, recent studies have proposed the use of the stack and draw method for engineering the optical properties of soft glasses, thus making it possible to manufacture GRIN specialty optical fibers [13]. In this context, it is worth mentioning that such GRIN specialty fibers have been used for the experimental demonstration of different nonlinear phenomena, such as quasi-periodic pulse breathing [14] and spatial beam self-cleaning [15], which provide indirect proofs of the presence of a parabolic refractive index profile.

To the contrary, direct measurements of the refractive index profile of nanostructured non-silica glass fibers remain a non-trivial task. As a matter of fact, soft glass fibers are manufactured with quite small variations of the doping concentration between core and cladding, which are poorly detectable with standard techniques, such as EDX spectroscopy. Moreover, being the stack and draw technique at the frontier of the manufacturing of specialty optical fibers, achieving complete control of fiber material properties during fiber drawing might be burdensome. Therefore, one

naturally wonders how to characterize soft glass GRIN fibers, and whether there is a way to measure the refractive index along the fiber axis after fiber drawing.

Such a task, which might sound rather challenging when using standard techniques (for instance, EDX spectroscopy only provides information in the vicinity of the fiber facet), may become feasible by recurring to X-ray computed microtomography (μ CT). At variance with electron spectroscopy, μ CT exploits the X-ray absorption contrast of the different constituents of a given sample. This allows for obtaining a full 3D map of the material density, which is determined by the doping concentration, that is proportional to the material refractive index [16]. Therefore, the μ CT intensity (I_μ) at X-ray frequencies takes the shape of n at optical frequencies, i.e.,

$$I_\mu \propto n. \quad (1)$$

For instance, μ CT enables us to determine the convexity factor of parabolic GRIN fibers, as discussed in [16] for standard silica fibers. We underline that (1) strictly holds in the absence of effects such as X-ray refraction and diffraction, i.e., when I_μ is purely determined by the material absorption [17]. This is, indeed, the case of optical fibers, as long as one limits the analysis of μ CT images to the region close to the fiber axis, i.e., far from the core/cladding interface.

Interestingly, the X-ray cross-section scales nonlinearly with Z [18]. As a result, it follows that μ CT is much more effective for materials made with heavy elements, such as soft glass materials. Unlike EDX spectroscopy, μ CT is unaffected by fiber bending or coating, and it does not require an in-vacuum environment to work. Furthermore, μ CT can be applied to optical fibers even in the presence of a plastic jacket, which, instead, has to be removed when using optical reflectometry and optical tomography [19,20]. The catch is that μ CT is much slower than conventional techniques, such as EDX spectroscopy.

To date, μ CT analyses have only been performed for silica fibers. In particular, μ CT analyses of photonic crystal, standard multimode fibers, and their preforms have been reported [16,21,22]. Moreover, in a recent work, μ CT was applied to visualize the shape of laser-induced damages in multimode optical fibers [23].

In this work, we report, we believe for the first time, the applicability and effectiveness of μ CT to specialty optical fibers. In particular, we focus our attention on soft glass optical fibers with step-index and GRIN profiles. Our results demonstrate that μ CT permits to obtain a 3D map of the refractive index profile of the fiber core. We found that soft glass fibers are more suitable than silica fibers for μ CT, e.g., they require shorter acquisition times, owing to their higher absorption by high Z chemical elements. In the case of GRIN fibers, we retrieved the parabolic profile of the refractive index even for samples with such a low doping concentration that their EDX traces remained flat. Our results prove that μ CT may provide a powerful tool for quality control and characterization of soft glass fibers.

2. Methods and materials

Our μ CT facility is composed of a microfocus source (Hamamatsu L12161-07, having focal spot size of 5 μ m), a motorized sample holder, and a flat panel detector (Hamamatsu C7942SK-05, whose pixel size is 50 μ m). A conical polychromatic X-ray beam was emitted with an aperture angle of 43°, and a focal spot of 5 μ m. The beam power was 10 W, and the X-ray tube voltage was set to 60 kV. The μ CT images were reconstructed by means of the Feldkamp-Davis-Kress back-projection algorithm [24]. All of the images reported in this work are produced by means of both Fiji and Avizo software for image analysis and visualization [25]. In all experiments, the distance between the source and the sample was 7 cm; whereas the distance between source and detector was 77 cm. The demagnified pixel was, thus, about 5 μ m, i.e., very close to the focal spot size.

The measurement time (which was of the order of 10 hours per sample as we collected a radiography every 0.1° over 3600°) corresponded to a dose of exposition of the fibers of about 2

kGy. As such, we did not observe any reduction of the fiber transmission after exposure. As a matter of fact, a dose of 2 kGy is about one order of magnitude smaller than the value that is required for inducing X-ray absorption-induced attenuation of the fiber optical transmission [26,27]. In this sense, μ CT provides a non-destructive tool for the characterization of optical fibers. However, we emphasize that whenever gamma-rays are used, a dose as high as 2 kGy may induce modifications of the fiber material structure [28]. The soft glass fiber samples investigated in this work were also subjected to EDX measurements. In order to increase the resolution and stability of the images, the fiber samples were first coated by using a manual sputterer (Agar Scientific AGB7340). The continuous conductive layer used for the coating consisted of 7 nm of gold. After this step, the samples were inserted into a desktop scanning electron microscope (Thermo Scientific Phenom ProX). The EDX data was gathered using a backscattered electron detector at 20 kV.

A list of tested fibers is reported in Table 1. We used two spans of commercial soft glass step-index fiber, which were made by different manufacturers (samples A and B), as well as two spans of in-house made soft glass GRIN fibers (samples C and D). Finally, we used standard fibers (samples E, F, and G), in order to compare silica and non-silica fibers. We underline that samples E-G are the same fibers that were used in Ref. [16]. However, we did not use the data of that work. Indeed, in order to make a fair comparison, we repeated the μ CT measurements of samples E-G within the same experimental conditions of samples A-D.

Table 1. List of optical fiber samples used in this work.

Sample	Type	Preform manufacture	Manufacturer	Description	Label [Ref.]
A	STEP	CVD	Thorlabs	ZrF ₄	ZBLAN 100/190 [29]
B	STEP	CVD	Verre Fluoré	ZBLAN	ZFG 90/150 [30]
C	GRIN	Stack and draw	University of Warsaw	Boron-silicate	NC34/NC42 [31,32]
D	GRIN	Stack and draw	University of Warsaw	Lead-bismuth-gallate	PBG [15]
E	STEP	CVD	Thorlabs	Pure silica core	FG050LGA [33]
F	GRIN	CVD	Alcatel	Ge-doped silica core	BI-MMF 50/125 [34]
G	GRIN	CVD	Thorlabs	Ge-doped silica core	GIF50E [35]

3. Results

Let us now illustrate the experimental results. First, we report on fiber characterization using EDX spectroscopy. Then, we show and analyze the μ CT images of soft glass fibers. Finally, we compare the results of μ CT for both silica and non-silica fibers.

3.1. Energy disperse X-ray spectroscopy

We carried out EDX measurements on all samples of Table 1, except for sample E. Here, however, we limit ourselves to showing the results for non-silica fibers. The EDX traces of standard fibers can be readily found elsewhere in the literature (see, for instance, Ref. [36]). In Fig. 1(a-d) we show the scanning electron microscope (SEM) images from samples A-D. As can be seen, the two step-index fibers (samples A and B) are made with different materials. Specifically, in sample A the concentrations of fluorine, lanthanum, and zirconium are practically identical between core and cladding (see the EDX trace in Fig. 1(a1)); the higher refractive index of the core with respect to the cladding is obtained by using a different concentration of barium and lead (see Fig. 1(a2)). On the other hand, in sample B the difference between core and cladding is due to a variation in the concentration of barium, zirconium, and hafnium, respectively. In both cases, a clear step-index profile can be identified. Whereas, as far as sample C is concerned, we may clearly see in Fig. 1(c1-c3) the parabolic profile of the concentration of elements such as oxygen, barium,

lead, and potassium: such a parabolic doping distribution is the fingerprint of a GRIN fiber. On the other hand, the GRIN refractive index profile of sample D is not evident from the EDX traces in Fig. 1(d1-d3). Indeed, besides cadmium and zinc, which are the elements with the lowest concentration (cfr. Figure 1(d3)), the parabolic profile of all other components is not evident from Fig. 1(d1-d2). Nevertheless, we should mention that the fiber spans, that were cleaved from the same spool of sample D, have previously been used for demonstrating beam self-cleaning (see Ref. [15]). This effect is greatly facilitated by the presence of a parabolic refractive index profile, which enhances mode mixing via quasi-phase-matched four-photon processes [37].

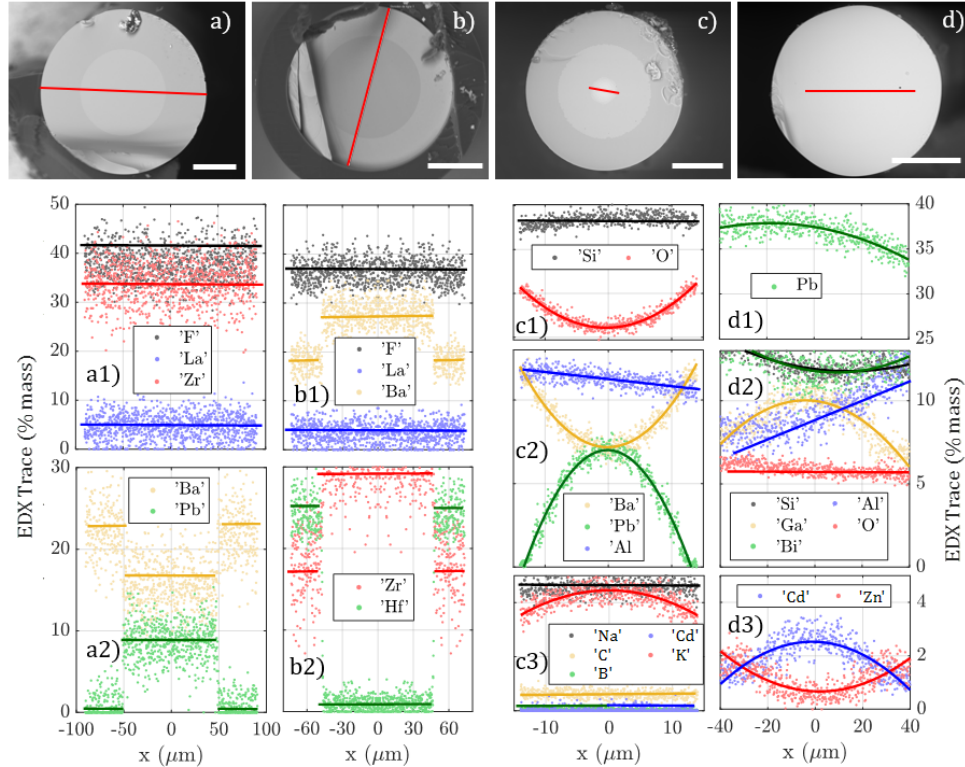


Fig. 1. (a-d) Scanning electron microscope images of samples A-D, respectively. (a1-d3) EDX traces taken along the red lines in (a-d). The white bars in (a-d) are 50 μm long.

3.2. Tomographic images of soft glass fibers

The 3D renderings of μCT images of samples A-D are shown in Fig. 2(a-d). Here we used a red (blue) color scale for step-index (GRIN) fibers. The peculiarities of samples A-D can be visually appreciated from their single tomographic slices, which are shown in Figs. 2(e-h), respectively. Note that, although the samples are nominally translationally invariant, we avoided averaging over the fiber axis, since this operation may be affected by possible inhomogeneities of the detector sensitivity. The μCT intensity profiles, $I_\mu(x)$, taken along the diameters of the slices in Fig. 2(e-h) are shown in Fig. 2(i-l), respectively. As it can be seen, for step-index fibers $I_\mu(x)$ remains nearly flat near the center of the fiber core, i.e., $|x| \approx 0$. Whereas, far from the fiber axis one observes a pronounced variation of $I_\mu(x)$, which we label as Δ . This variation is associated with the density difference between core and cladding (hence, with their refractive index difference). We emphasize such variations in the insets of Fig. 2(i,j). On the other hand, I_μ

has a parabolic profile in the vicinity of the axis of GRIN fibers, as indicated by the parabolic fit in the inset of Fig. 2(k-l).

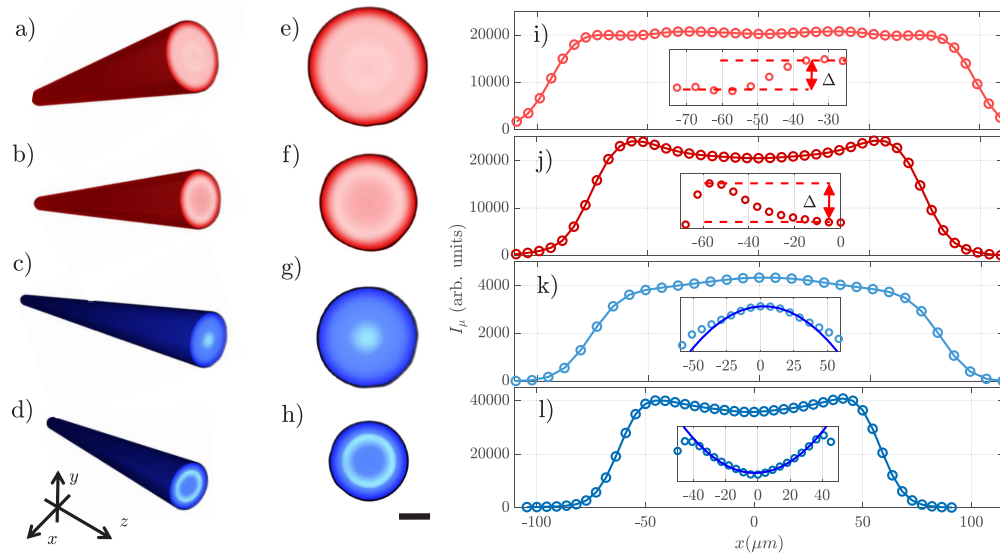


Fig. 2. Results of μCT measurements on soft glass fibers. (a-d) 3D rendering of the μCT intensity I_μ for samples A-D, respectively. (e-f) Single slices of (a-d). (i-l) I_μ profile extracted along the diameter of (e-h). The insets show the details of the core/cladding interface (i,j) and the core center (k,l). On the bottom of (d) the reference system is illustrated, whose origin is on the fiber axis, which is parallel to the z-direction for all fibers. The black bar at the bottom of (h) is $50 \mu\text{m}$ long and is the reference for (e-h).

Now, it should be clarified that only the *shape* of I_μ reflects the profile of n , because of the relationship of linear proportionality between these two quantities [cfr Eq. (1)]. Therefore, I_μ might either increase or decrease when approaching the fiber axis, i.e., where n always has its maximum. These two opposite cases are represented in Fig. 2(k and l), respectively. In any case, I_μ maintains the same parabolic shape of n inside the fiber core. Analogously, in the case of step-index fibers, one may find that the cladding is associated with either a lower or a higher value of I_μ with respect to its value in the core, regardless of the fact that the core refractive index is always higher in the core than in the cladding. The former case is that of Fig. 2(i), where I_μ mimics the expected profile of n , i.e., it is higher in the core and lower in the cladding (cfr. the detail of the core/cladding interface in the inset of Fig. 2(i)). On the other hand, Fig. 2(j) shows that the variation of I_μ at the core/cladding interface has an opposite trend with respect to n : namely, I_μ turns out to be higher in the cladding than in the core (see the inset of Fig. 2(j)).

The different behavior of I_μ (i.e., whether it increases or decreases in the same way as n when one moves away from the fiber axis) depends on the fiber manufacturing process, i.e., on the core and cladding materials. Samples A and B provide relevant examples. In the former, the higher refractive index of the core with respect to the cladding is obtained by replacing barium ($Z = 56$) with lead ($Z = 82$), as indicated in Fig. 1(a2). Since the X-ray cross section grows larger with Z , it is straightforward to understand that I_μ , which is somehow a measurement of the X-ray absorption, will be higher in the core than in the cladding in this case (Fig. 2(i)). On the other hand, in sample B the core/cladding refractive index difference is produced by replacing hafnium ($Z = 72$) with zirconium ($Z = 40$), as it can be seen in Fig. 1(b2). As a consequence, in the core I_μ is lower than in the cladding (Fig. 2(j)). A similar situation occurs for samples D and C. However, in the former, the link between I_μ and the chemical composition is not as easy to determine as in

other samples. This is because, as previously mentioned, in sample D the chemical composition variation between core and cladding is relatively tiny. Nonetheless, our μ CT facility was still capable of capturing the parabolic shape of I_μ (and thus of n) in the core. In this sense, μ CT turns out to be more effective than EDX in retrieving the refractive index profile of the fiber core.

In the last part of this section, we will return to the crucial aspect of the relationship between I_μ and Z , when comparing the effectiveness of μ CT when applied to soft glasses and silica fibers. Now, we just take a little step back, in order to verify the reliability of our μ CT facility by quantitatively analyzing the results of Fig. 2.

3.3. Analysis of the μ CT images

As we have seen in the previous subsection, the shape of the μ CT traces in Fig. 2(i-l) qualitatively corresponds to the expected refractive index profile. This constitutes the major finding of this work. Before continuing with our analysis, it is appropriate to discuss the limitations of our μ CT facility, with the purpose of assessing the reliability of our measurements. The main issue of μ CT, when applied to optical fibers, is its limited spatial resolution, which is determined by the focal spot size of the X-ray source. Although cutting-edge synchrotron beamlines and nanotomography facilities may allow for resolving sub-micrometric spatial features, so that one may characterize singlemode fibers, our present spatial resolution is about 5 μ m. This means that, when applied to a standard fiber with a 50 μ m core diameter, we are limited to measuring up to ten data points in the I_μ profile (cfr. the insets of Fig. 2(k,l)). Therefore, one may naturally wonder whether our μ CT facility can properly resolve the spatial (and thus the "optical") features of our fibers. In order to verify this issue, we compared the diameters of the fibers' core and cladding, as measured with SEM, with those retrieved by μ CT. The result is shown in Table 2, where we report the values of the diameters provided by the manufacturer (nominal values), those measured by SEM, and by μ CT, respectively. As can be seen, we found a quite good agreement among nominal and measured values: the values of the diameters retrieved by μ CT differ by less than twice the spatial resolution from the nominal and SEM/EDX-measured values (note that the experimental values of SEM/EDX and μ CT are approximated to 1 μ m for easier comparison). We emphasize that the agreement with the nominal and the SEM/EDX-measured values of the fiber core and cladding diameters proves that the parabolic shape of I_μ of GRIN fibers is not due to beam hardening effects.

Table 2. Comparison of the core/cladding diameters measured by μ CT, with the values provided by the manufacturer (nominal), and the values retrieved by the SEM/EDX. In the case of sample C, we report three values, since that fiber has a double cladding structure (cfr. Figure 1(c)).

Diameters (μ m)			
Sample	Nominal	SEM/EDX	μ CT
A	100 \pm 2 / 190 \pm 2.5	101/193	94/192
B	90/150	92/150	88/151
C	/	28/90/160	22/102/154
D	/	80/125	68/118
E	50 \pm 1 / 125 \pm 2	/	47/120
F	50 \pm 2.5 / 125 \pm 2	47/125	42/120
G	50 \pm 2.5 / 125 \pm 1	51/120	42/120

The procedure for determining the core and cladding diameters from μ CT is illustrated in Fig. 3. Here we show the case of one of the step-index fibers, i.e., of sample B, (Fig. 3(a-c)) and

of one of the GRIN fibers, i.e., sample D, (Fig. 3(d-f)). The curves in Fig. 3(a,d) are the same as those in Fig. 2(j,l), respectively, besides their normalization to the maximum of intensity. The curves in Fig. 3(b,e and c,f) represent the trend of the first and the second derivative of I_μ with respect to x , which we dub as I'_μ and I''_μ , respectively.

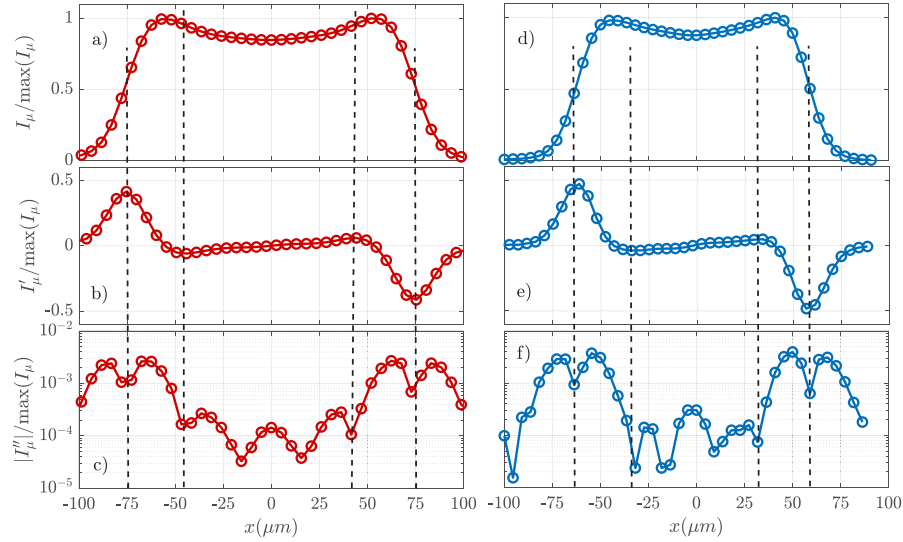


Fig. 3. Analysis of the μ CT intensity profile of sample B (a-c) and D (d-f), for the determination of the core and cladding diameters.

Specifically, in Fig. 3(c,f) we show the absolute value of I''_μ : we use a logarithmic scale in order to emphasize the inflection points of the curves in Fig. 3(a,d). The latter indicates the presence of an interface between two different materials. Indeed, for each curve, we found four inflection points, which are highlighted by vertical dashed lines in the figures. These inflections are due to the core/cladding and the cladding/air interfaces, whose measured distances provide the values of the fiber core and cladding that we reported in Table 3. As a side note, we emphasize that the inflection points of I_μ correspond to either maxima or minima of I'_μ , i.e., to zeros of I''_μ . Now, when analyzing the μ CT profiles, we found that I''_μ has several "zeros" (cfr., the minima in Fig. 3(c,f) at $|x| \approx 0$). However, some of them, e.g., those providing values of $|I''_\mu|/\max(I_\mu) < 10^{-4}$ in Fig. 3(c), are ascribable to experimental measurement errors, which introduce small fluctuations in the μ CT intensity.

3.4. Comparison with silica fibers

The previously discussed estimation of the core and cladding diameters only takes into account the relative μ CT intensities. In other words, in Fig. 3 we considered the profiles of I_μ which are normalized to their maximum value. Nevertheless, one may notice in Fig. 2(i-l) that the μ CT intensity values are lower for sample C than for all other samples. This is because sample C contains elements such as boron, which are lighter than the elements of the other soft glasses that we used in this work (cfr. Figure 1).

In this last section, we discuss the experimental measurements of I_μ for the different fibers, with the aim of comparing the effectiveness of μ CT when applied to either soft glass fibers (samples A-D) or to standard silica fibers (samples E-G). The easiest way to compare our samples in terms of their response to μ CT, is to consider the values of I_μ on the fiber axis, i.e., at $x = y = 0$.

It is also convenient to define an effective value of the atomic number (Z_{eff}) as follows

$$Z_{\text{eff}}(x) = \sum_i Z_i \cdot [X_i](x), \quad (2)$$

where the index i runs over the elements which compose the fiber core material. Each element has an x -dependent concentration $[X_i](x)$, which can be retrieved from the EDX traces in Fig. 1.

The measured values of I_μ on the axis of all fibers are shown in a log-log plot vs. Z_{eff} in Fig. 4(a). Owing to the presence of high Z elements, the μCT intensity associated with soft glasses is higher than in silica. The log-log plot, in particular, allows for spotting an empirical relationship between I_μ and Z_{eff} . As can be seen in Fig. 4(a), the experimental points appear to be aligned: the corresponding dot-dashed black curve is the fitting curve law

$$I_\mu = \alpha Z_{\text{eff}}^N, \quad (3)$$

where α is a constant, and N takes into account the nonlinearity of the relationship between I_μ and Z_{eff} . We found that the slope of the dot-dashed line in Fig. 4(a) is $N \simeq 2$.

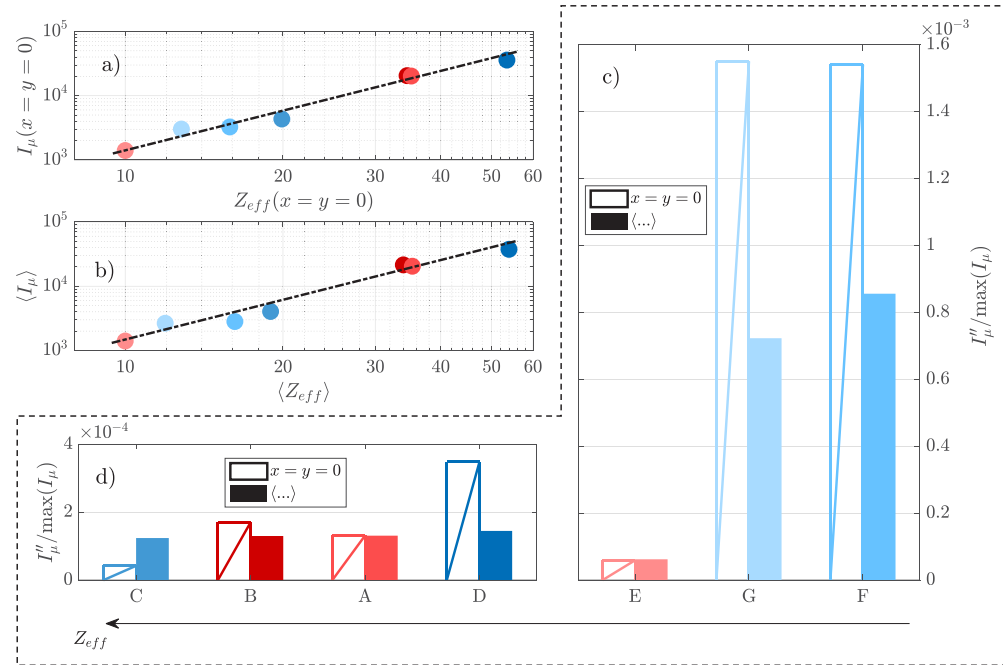


Fig. 4. Comparison between soft glass and silica fibers in terms of their μCT response. (a,b) μCT intensity on the fiber axis (a) and averaged over the fiber core (b) vs. the effective atomic number Z_{eff} . (c) Values of the second derivative of the μCT intensity for silica fibers, sorted by Z_{eff} . (d) Same as (c) for non-silica fibers.

In order to test the validity of the empiric relationship (3), we used this equation to fit the values of I_μ and Z_{eff} , averaged over the fiber core: $\langle I_\mu \rangle$ and $\langle Z_{\text{eff}} \rangle$. Here the averaging $\langle \dots \rangle$ is defined as

$$\langle \xi \rangle = \frac{1}{2x_c} \int_{-x_c}^{x_c} \xi(x) dx, \quad (4)$$

where ξ a function of x , and x_c is the radius of the fiber core. Interestingly, even in this case, we obtained $N \simeq 2$. Indeed, the fitting lines in both Fig. 4(a) and (b) are parallel. This result indicates

that a quadratic-like relationship holds between I_μ and Z_{eff} . In other words, if two samples have a ratio of Z_{eff} equal to 2, the fiber composed with heavier elements would require about 1/4 of time in order to provide the same value of μCT intensity as the other one. This aspect, which might seem trivial at first sight, turns out to be rather important. One has to remember that, within our experimental setup, each silica sample required as much as 10 hours of acquisition time. Saving acquisition time permits, on the one hand, reducing the degradation of the X-ray detector and, on the other hand, decreasing the cost of a single tomography. Clearly, both aspects are crucial for the possible application of μCT to the characterization of optical fibers at the industrial level.

Finally, let us compare the values of I''_μ that were measured in the core of our samples. The second derivative of the μCT intensity is particularly interesting for GRIN fibers since its value on the fiber axis is proportional to the core/cladding refractive index difference [16]. In the case of step-index fibers, instead, I''_μ is expected to be close to zero across the entire fiber core, since their refractive index profile is ideally flat. Consistently, in the case of GRIN silica fibers, I''_μ is about ten times higher than in step-index silica fibers (see Fig. 4(c)). Note that we kept the same color code (red and blue colors associated with step-index and GRIN fibers, respectively) as in Fig. 2 and 3. On the other hand, in the case of soft glasses, the difference between step-index and GRIN fibers is not so pronounced (see Fig. 4(d)). For instance, I''_μ on the axis of sample C is even lower than in step-index fibers (cfr. empty bars in Fig. 4(c)). This discrepancy is ascribable to the low resolution of our μCT facility (the core diameter of fiber C is only about 25 μm as reported in Table 2). In the case of sample D, instead, we found that $\langle I''_\mu \rangle$ has practically the same value as in step-index fibers, although it is a GRIN fiber (cfr. full bars in Fig. 4(d)). However, the value of I''_μ on the fiber axis is twice that of step-index soft glass fibers (cfr. empty bars in Fig. 4(d)). Once again, this indicates that μCT is capable of detecting the graded shape of the refractive index of sample D, whose core and cladding materials only differ by a small variation of the doping concentration (cfr. Figure 1(d1-d3)).

4. Conclusion

In this work, we have introduced the μCT technique for the characterization of specialty optical fibers. We experimentally demonstrated that μCT is able to resolve the shape of the refractive index of soft glass optical fibers. Specifically, we successfully characterized both commercially available and in-house-made specialty optical fibers for mid-infrared applications. We have successfully verified the accuracy of our μCT measurements: in spite of a low spatial resolution μCT facility, the geometrical features of all fibers were accurately determined. We found an excellent agreement between the values of core and cladding diameters measured via μCT , those measured by means of SEM and EDX spectroscopy, and the fiber manufacturer specifications.

When compared with standard silica fibers, the presence of high atomic number elements in soft glasses makes specialty fibers comparatively more suitable for their characterization via μCT . Indeed, high-atomic-number elements are responsible for higher X-ray absorption. This allows to save energy and time, as well as to increase the detector lifetime. In particular, we empirically found that the intensity of μCT images (which is inversely proportional to the acquisition time) scales quadratically with the effective atomic number of the core material. In this regard, our results pave the way for the application of μCT to efficiently characterize novel types of optical fibers, whose refractive index profile remains otherwise challenging to determine when using standard techniques.

Funding. European Research Council (740355); the European Union under the Italian National Recovery and Resilience Plan (NRRP) of NextGenerationEU, partnership on ‘Telecommunications of the Future’ (PE00000001—program ‘RESTART’) Ministero dell’Università e Ricerca (PIR01-00008, R18SPB8227); Agence Nationale de la Recherche (10-LABX-0074-01, 18-CE080016-01); Fundacja na rzecz Nauki Polskiej (TEAM NET POIR.04.04.00-00-1644/18).

Acknowledgments. We would like to thank Katarzyna Krupa and Oreste De Luca for fruitful discussions.

Disclosures. The authors declare no conflict of interest.

Data availability. Data underlying the results presented in this paper are not publicly available at this time but may be obtained from the authors upon reasonable request.

References

1. S. R. Nagel, J. B. MacChesney, and K. L. Walker, "An overview of the modified chemical vapor deposition (mcvd) process and performance," *IEEE Trans. Microwave Theory Tech.* **30**(4), 305–322 (1982).
2. C. Chen and Y. Jaluria, "Effects of doping on the optical fiber drawing process," *Int. J. Heat Mass Transfer* **52**(21-22), 4812–4822 (2009).
3. T. Hansson, A. Tonello, T. Mansuryan, F. Mangini, M. Zitelli, M. Ferraro, A. Niang, R. Crescenzi, S. Wabnitz, and V. Couderc, "Nonlinear beam self-imaging and self-focusing dynamics in a grin multimode optical fiber: theory and experiments," *Opt. Express* **28**(16), 24005–24021 (2020).
4. K. Krupa, A. Tonello, A. Barthélémy, V. Couderc, B. M. Shalaby, A. Bendahmane, G. Millot, and S. Wabnitz, "Observation of geometric parametric instability induced by the periodic spatial self-imaging of multimode waves," *Phys. Rev. Lett.* **116**(18), 183901 (2016).
5. K. Krupa, A. Tonello, B. M. Shalaby, M. Fabert, A. Barthélémy, G. Millot, S. Wabnitz, and V. Couderc, "Spatial beam self-cleaning in multimode fibres," *Nat. Photonics* **11**(4), 237–241 (2017).
6. C. D. Marciniak, H. B. Ball, A. T.-H. Hung, and M. J. Biercuk, "Towards fully commercial, uv-compatible fiber patch cords," *Opt. Express* **25**(14), 15643–15661 (2017).
7. G. P. Agrawal, "Nonlinear fiber optics," in *Nonlinear Science at the Dawn of the 21st Century*, (Springer, 2000), pp. 195–211.
8. P. Werle, F. Slemr, K. Maurer, R. Kormann, R. Mücke, and B. Jänker, "Near-and mid-infrared laser-optical sensors for gas analysis," *Opt. Lasers Eng.* **37**(2-3), 101–114 (2002).
9. C. R. Petersen, U. Møller, I. Kubat, *et al.*, "Mid-infrared supercontinuum covering the 1.4–13.3 μm molecular fingerprint region using ultra-high na chalcogenide step-index fibre," *Nat. Photonics* **8**(11), 830–834 (2014).
10. L. Shi and R. R. Alfano, *Deep imaging in tissue and biomedical materials: using linear and nonlinear optical methods* (CRC Press, 2017).
11. W. Wang, B. Zhou, S. Xu, Z. Yang, and Q. Zhang, "Recent advances in soft optical glass fiber and fiber lasers," *Prog. Mater. Sci.* **101**, 90–171 (2019).
12. V. R. K. Kumar, A. George, W. Reeves, J. Knight, P. S. J. Russell, F. Omenetto, and A. Taylor, "Extruded soft glass photonic crystal fiber for ultrabroad supercontinuum generation," *Opt. Express* **10**(25), 1520–1525 (2002).
13. R. Buczyński, M. Klimczak, T. Stefaniuk, R. Kasztalanic, B. Siwicki, G. Stępniewski, J. Cimek, D. Pysz, and R. Stępień, "Optical fibers with gradient index nanostructured core," *Opt. Express* **23**(20), 25588–25596 (2015).
14. T. Karpate, G. Stępniewski, T. Kardaś, D. Pysz, R. Kasztalanic, Y. Stepanenko, R. Buczyński, K. Krupa, and M. Klimczak, "Quasi-periodic spectro-temporal pulse breathing in a femtosecond-pumped tellurite graded-index multimode fiber," *Opt. Express* **31**(8), 13269–13278 (2023).
15. Z. Eslami, L. Salmela, A. Filipkowski, D. Pysz, M. Klimczak, R. Buczynski, J. M. Dudley, and G. Genty, "Two octave supercontinuum generation in a non-silica graded-index multimode fiber," *Nat. Commun.* **13**(1), 2126 (2022).
16. M. Ferraro, M. C. Crocco, F. Mangini, *et al.*, "X-ray computed μ -tomography for the characterization of optical fibers," *Opt. Mater. Express* **12**(11), 4210–4222 (2022).
17. Z. H. Levine, E. J. Garboczi, A. P. Peskin, A. A. Ekman, E. Mansfield, and J. D. Holm, "X-ray computed tomography using partially coherent fresnel diffraction with application to an optical fiber," *Opt. Express* **29**(2), 1788–1804 (2021).
18. C. Davission, "Interaction of γ -radiation with matter," in *Alpha-, Beta-and Gamma-Ray Spectroscopy*, (Elsevier, 1968), pp. 37–78.
19. W. Stewart, "Optical fiber and preform profiling technology," *IEEE Trans. Microwave Theory Tech.* **30**(10), 1439–1454 (1982).
20. S. Fan, S. Smith-Dryden, J. Zhao, S. Gausmann, A. Schülzgen, G. Li, and B. E. Saleh, "Optical fiber refractive index profiling by iterative optical diffraction tomography," *J. Lightwave Technol.* **36**(24), 5754–5763 (2018).
21. T. Sato, O. Ikeda, Y. Yamakoshi, and M. Tsubouchi, "X-ray tomography for microstructural objects," *Appl. Opt.* **20**(22), 3880–3883 (1981).
22. S. Sandoghchi, G. Jasion, N. Wheeler, *et al.*, "X-ray tomography for structural analysis of microstructured and multimaterial optical fibers and preforms," *Opt. Express* **22**(21), 26181–26192 (2014).
23. M. Ferraro, F. Mangini, Y. Sun, *et al.*, "Multiphoton ionization of standard optical fibers," *Photonics Res.* **10**(6), 1394–1400 (2022).
24. L. A. Feldkamp, L. C. Davis, and J. W. Kress, "Practical cone-beam algorithm," *J. Opt. Soc. Am. A* **1**(6), 612–619 (1984).
25. J. Schindelin, I. Arganda-Carreras, E. Frise, V. Kaynig, M. Longair, T. Pietzsch, S. Preibisch, C. Rueden, S. Saalfeld, B. Schmid, J.-Y. Tinevez, D. J. White, V. Hartenstein, K. Eliceiri, P. Tomancak, and A. Cardona, "Fiji: an open-source platform for biological-image analysis," *Nat. Methods* **9**(7), 676–682 (2012).
26. S. Girard, J. Kuhnenn, A. Gusarov, B. Brichard, M. Van Uffelen, Y. Ouerdane, A. Boukenter, and C. Marcandella, "Radiation effects on silica-based optical fibers: Recent advances and future challenges," *IEEE Trans. Nucl. Sci.* **60**(3), 2015–2036 (2013).

27. D. Di Francesca, A. Boukenter, S. Agnello, S. Girard, A. Alessi, P. Paillet, C. Marcandella, N. Richard, F. Gelardi, and Y. Ouerdane, "X-ray irradiation effects on fluorine-doped germanosilicate optical fibers," *Opt. Mater. Express* **4**(8), 1683–1695 (2014).
28. S. Girard, J. Keurinck, A. Boukenter, J.-P. Meunier, Y. Ouerdane, B. Azais, P. Charre, and M. Vié, "Gamma-rays and pulsed x-ray radiation responses of nitrogen-, germanium-doped and pure silica core optical fibers," *Nucl. Instrum. Methods Phys. Res., Sect. B* **215**(1-2), 187–195 (2004).
29. 285 nm - 4.5 μm Transmission Range; 0.2035 NA and 93% Transmission at 2.5 μm ; https://www.thorlabs.com/newgrouppage9.cfm?objectgroup_id=7062.
30. 0.3 μm - 4.5 μm Transmission Range; 0.15 NA and < 10 dB/km losses at 2.5 μm ; <https://leverfluore.com/scientific-world/fluoride-fibers/general-properties/>.
31. R. Kasztelanica, A. Filipkowski, A. Anuszkiewicz, P. Stafiej, G. Stępniewski, D. Pysz, K. Krzyżak, R. Stepień, M. Klimczak, and R. Buczynski, "Integrating free-form nanostructured grin microlenses with single-mode fibers for optofluidic systems," *Sci. Rep.* **8**(1), 5072 (2018).
32. A. Filipkowski, H. T. Nguyen, R. Kasztelanica, T. Stefaniuk, J. Cimek, D. Pysz, R. Stepień, K. Krzyżak, P. Karioja, and R. Buczynski, "Development of large diameter nanostructured grin microlenses enhanced with temperature-controlled diffusion," *Opt. Express* **27**(24), 35052–35064 (2019).
33. <https://www.thorlabs.com/thorproduct.cfm?partnumber=FG050LGA>.
34. https://www.prysmiangroup.com/sites/default/files/business_markets/markets/downloads/datasheets/MMF—Graded-Index-Multimode-Optical-Fiber-50_125-m_0.pdf.
35. <https://www.thorlabs.com/thorproduct.cfm?partnumber=GIF50E>.
36. F. Mangini, M. Ferraro, M. Zitelli, A. Niang, A. Tonello, V. Couderc, and S. Wabnitz, "Multiphoton-absorption-excited up-conversion luminescence in optical fibers," *Phys. Rev. Appl.* **14**(5), 054063 (2020).
37. M. Ferraro, F. Mangini, M. Zitelli, and S. Wabnitz, "On spatial beam self-cleaning from the perspective of optical wave thermalization in multimode graded-index fibers," *arXiv*, arXiv:2304.12006 (2023).